Applied Catalysis B: Environmental 160–161 (2014) 44–50

Contents lists available at ScienceDirect

Applied Catalysis B: Environmental

journal homepage: www.elsevier.com/locate/apcatb

Dramatic visible activity in phenol degradation of TCNQ@TiO_2 photocatalyst with core–shell structure

Wenjun Jiang, Mo Zhang, Jun Wang, Yanfang Liu, Yongfa Zhu *

Department of Chemistry, Tsinghua University, Tsinghua Yuan, Beijing 100084, PR China

ARTICLE INFO

Article history:
Received 17 February 2014
Received in revised form 22 April 2014
Accepted 27 April 2014
Available online 4 May 2014

Keywords:
Visible activity
Core–shell structure
Phenol degradation
TCNQ
TiO_2

ABSTRACT

TCNQ@TiO_2 visible photocatalyst with core–shell structure was synthesized by adsorption methods. The photocatalytic activity was adjusted by the thickness of the shell. After formation of TCNQ@TiO_2 core–shell structure, visible light photoactivity can be obtained. The photocatalyst activity of TCNQ@TiO_2 was enhanced gradually with the increasing proportion of TCNQ. When the mass fraction of TCNQ reaches 20%, it exhibits the highest visible activity. The apparent rate constant k of TCNQ@TiO_2-20% is 0.2583 h^{-1}, which is almost 67.9 times as high as that of pure TiO_2. Under visible irradiation, the photogenerated holes on the HOMO orbit of TCNQ can be injected into the VB of TiO_2, resulting in the oxidation of organic pollutant directly. However, the energy of the holes injected into the VB of TiO_2 is not high enough to mineralize phenol completely. Under UV irradiation, the photogenerated electrons on the CB of TiO_2 can be injected into the LUMO orbit of TCNQ, which is too low that electrons could not combine with O_2 easily, interdicting the formation of superoxide radicals and resulting in the decrease of photoactivity.

1. Introduction

Photocatalytic technology has great application prospect in degradation of organic pollutant. However, the degradation performance is not so satisfactory in the process of actual pollutant treatment due to the low catalytic efficiency and poor visible light activity. Thus, the design of photocatalysts mainly concentrates on the following two aspects. One is how to restrain the recombination of photoinduced carriers and improve the efficiency of photocatalyst. Another is how to expand the absorption edge to absorb visible and even infrared light. As TiO_2 has the advantages of non-toxic, non-pollution, strong oxidation ability [1,2], it has been widely used in the treatment of wastewater containing low concentration of organic pollutant since Bard [3] oxidized CN^- into OCN^- with TiO_2 for the first time. However, the forbidden band of TiO_2 is far too wide (anatase is 3.2 eV, rutile is 3.0 eV) [4–6], which determines that it can only exhibit activity under ultraviolet radiation and its large-scale commercial application is restricted severely. At present the acquisition of visible activity of TiO_2 is mainly via the modification of TiO_2 to reduce the forbidden band width and expand the absorption edge of TiO_2 through photosensitive treatment [2,7–9], metal or nonmetal doping [10–15], surface modification of semiconductor or polymer [16–21] and noble metal modification [22–24]. However, the development of efficient TiO_2 photocatalyst with expanded absorption edge is still in progress.

7,7,8,8-Tetracyanoquinodimethane (TCNQ) is a neutral organic molecule, whose atoms are all in the same plane, and all the P electrons of C and N participate in the formation of P–π conjugation [25,26]. TCNQ can combine with other semiconductors to form charge transfer compounds [27–30]. These charge transfer compounds can absorb sunlight in almost the whole spectral range, which is pretty promising in terms of expanding absorption edge of semiconductors.

TCNQ@TiO_2 as a highly efficient visible photocatalyst with core–shell structure was synthesized via a facile method of adsorption and assembly in solution [20,31–35]. The method is very simple and could be used as a universal pathway to improve the activity of photocatalyst and applied in the environment remediation.

2. Experimental

2.1. Preparation of TCQN@TiO_2 photocatalyst

TCNQ was purchased from Beijing Chemical Reagent Corp, PR China; TiO_2 (P25) used to prepare TCNQ@TiO_2 photocatalysts was obtained from Degussa. All other reagents used in this research were analytical pure and used without further purification. The

* Corresponding author. Tel.: +86 10 62787601; fax: +86 10 62787601.
E-mail address: zhuyf@mail.tsinghua.edu.cn (Y. Zhu).

http://dx.doi.org/10.1016/j.apcatb.2014.04.050
0926-3373/

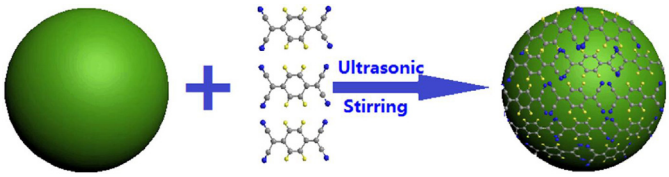

Scheme 1. Preparation of TCNQ@TiO_2 catalyst.

preparation of TCNQ@TiO_2 photocatalysts was as follows showed in Scheme 1: 1.25 g TCNQ was dissolves in 250 ml tetrahydrofuran (THF) to form 0.005 g/ml THF solution of TCNQ. Different volumes of TCNQ solution were measured and diluted to 100 ml with ethanol. 0.5 g TiO_2 was added into the above solution then the beaker sealed with plastic wrap was placed in an ultrasonic bath for 1 h. The mixture was vigorously stirring in the fume hood until the THF evaporated completely and then opaque powder was obtained. Different mass ratios of TCNQ@TiO_2 photocatalysts were prepared in the oven by the power evaporated at 150 °C for 4 h.

TiO_2 and TCNQ@TiO_2 electrodes were prepared by dipping coating method: 10 mg of photocatalyst was suspended in 1 ml ethanol to make a slurry, the slurry was then dip-coated onto a 2 cm × 4 cm indium-tin oxide glass electrode. The electrodes were then exposed to UV light for 12 h to eliminate ethanol and calcined at 150 °C for 1 h.

2.2. Characterization of TCQN@TiO_2 photocatalyst

High resolution transmission electron microscopy (HRTEM) images were obtained by JEM 2010F field emission transmission electron microscope with an accelerating voltage of 200 kV. The diffuse reflectance absorption spectra (DRS) of the samples were recorded in the range of 200–900 nm on a UV–vis spectrophotometer (Hitachi UV-3010) equipped with an integrated sphere attachment, and $BaSO_4$ was used as a reference. X-ray diffraction (XRD) patterns of the powders were recorded at room temperature by a Bruker D8 Advance X-ray diffractometer at 40 kV and 40 mA for monochromatized Cu $K\alpha$ ($\lambda = 1.5406$ Å) radiation. The Brunauer–Emmett–Teller (BET) specific surface area of the samples was characterized by nitrogen adsorption at 77 K with a Micromeritics 3020 instrument. Raman spectra were recorded on a microscopic confocal Raman spectrometer (HORIBA HR800) with an excitation of 514.5 nm laser light. Fourier transform infrared (FT-IR) spectra were carried out using Bruker V70 spectrometer in the frequency of 3100–800 cm^{-1} with a resolution of 1 cm^{-1}. Electrochemical and photoelectrochemical measurements were performed in a three-electrode quarts cells with 0.1 M Na_2SO_4 electrolyte solution. Platinum wire was used as counter and saturated calomel electrode (SCE) used as reference electrodes, respectively, and TCNQ@TiO_2 films electrodes on ITO served as the working electrode. The photoelectrochemical experiment results were recorded with an electrochemical system (CHI-660D, China).

2.3. Photocatalytic evaluation

The photocatalytic activities of the as-prepared samples were evaluated by the decomposition of phenol in solution in multi-tube agitated reactor (XPA-7). UV light source was obtained by a 300 W mercury lamp ($\lambda = 365$ nm) and the average light intensity was 1.315 mW/cm. 2.25 mg photocatalyst was added into prepared 50 ml 20 ppm phenol solution. Before the light irradiation, the suspensions were firstly ultrasonic dispersed in dark for 30 min, then magnetically stirred for 120 min to reach the adsorption–desorption equilibrium. At given time intervals, 2 ml aliquots were sampled and filtered with a microporemembrane. Synchronously, the filtrates of phenol solutions at different conditions were analyzed by recording variations of the phenol peak area. HPLC was adopted to detect phenol concentration and its degradation products distribution. Methanol and water (volume ratio: 60/40) were mobile phase, the elution time was 6 min, the flow rate was 1 ml/min, determine wavelength was 270 nm and chromatographic column was C18 reversed column (Agilent 1100, 4.6 nm × 200 nm). In addition, the visible light was provided by 500 W xenon lamp with 450 nm optical filters and the average visible light intensity was 23.6 mW/cm^2. The method was similar with the UV-light degradation above mentioned except that the concentration of phenol was 5 ppm.

3. Results and discussion

3.1. Photocatalytic activity

The photocatalytic activities of the TCNQ@TiO_2 samples for phenol degradation under visible light and UV light are shown in Fig. 1a and b. As can be seen in Fig. 1a, the pure TiO_2 show little activity in degrading phenol and the apparent rate constant k of pure TiO_2 is 0.0038 h^{-1} since TiO_2 could not be excited by visible light irradiation. The pure TCNQ exhibited no visible light activity either. Interestingly, the photocatalyst activity of TCNQ@TiO_2 was enhanced gradually with the increasing proportion of TCNQ. When the mass fraction of TCNQ reaches 20%, it exhibits the highest visible activity. The apparent rate constant k of TCNQ@TiO_2-20% is 0.2583 h^{-1}, which is almost 67.9 times as high as that of pure TiO_2. However, as the proportion of TCNQ further increases, the degradation rate decreases gradually though it remains higher than that of TiO_2. Although the visible light activity of TiO_2 was enhanced greatly, the UV activity of TiO_2 was not improved. As can be seen in Fig. 1b, all of the TCNQ@TiO_2 photocatalysts exhibited lower photocatalytic activity than the pure TiO_2 under UV light irradiation. The photocatalytic activity was decreased gradually with the increasing proportion of TCNQ. When the proportion of TCNQ reached 10%, the apparent rate constant k of the as-prepared photocatalyst was 0.003 min^{-1}, while the k of the pure TiO_2 was 0.022 min^{-1}, indicating that the intrinsic photocatalytic activity was restrained greatly.

Photocurrents of TCNQ@TiO_2 electrodes were measured to investigate the electronic interaction between TCNQ and TiO_2 (Fig. 1c and d). Photocurrents of TCNQ@TiO_2 (Fig. 1c) increased remarkably and then decreased with the increasing proportion of TCNQ. TCNQ@TiO_2-20% exhibited the highest photocurrent response, which was increased by two orders of magnitude compare to TiO_2. The increase of photocurrents indicates that the separation efficiency of photoinduced electrons and holes was enhanced greatly, which implies that there may be some interactions between TiO_2 and TCNQ. The photocurrent responses decreased gradually when the proportion of TCNQ was over 20%, which may be associated with the formation of bulk crystals of TCNQ. Excessive TCNQ resulted in low interaction between TiO_2 and TCNQ and the decrease of photocatalytic activity. As can be seen in Fig. 1d, the photocurrents under UV irradiation decreased with the increasing proportion of TCNQ. The photocurrent of TiO_2 was about 0.00012 Å, while TCNQ@TiO_2-5% showed almost no photocurrent responses, which indicates the separation of photoinduced electrons and holes was restrained greatly.

HPLC was utilized to investigate the changes of phenol and its degradation intermediates along with irradiation time. Fig. 2a shows the changes of phenol and its degradation intermediates with visible irradiation. The peak at 1.5 min was lower fatty acid, the peak at 2 and 2.5 min was TCNQ, the peak at 2.8 min was system peak, the peak at 3.4 min was hydroquinol, the peak at 4.2 min

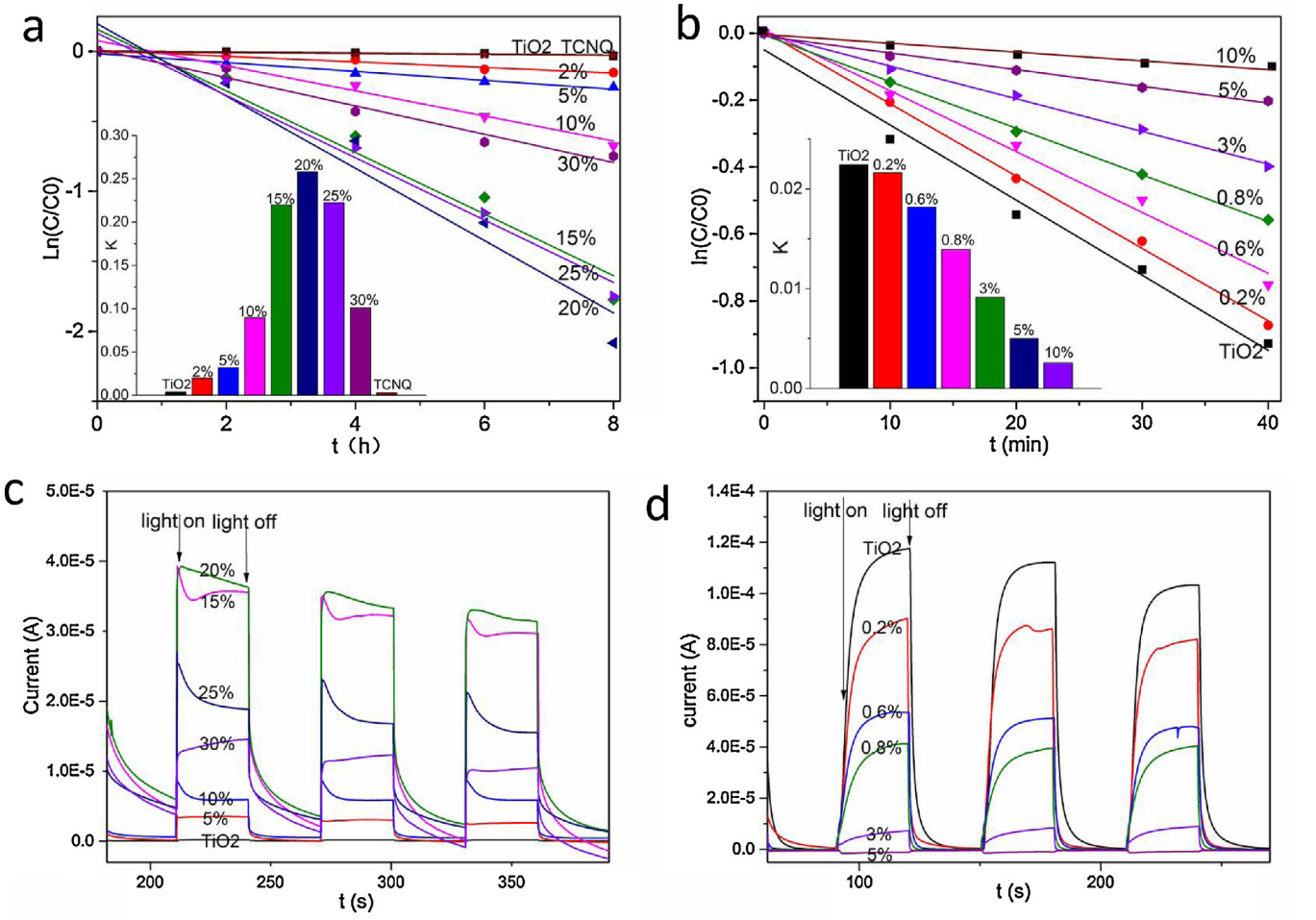

Fig. 1. Photocatalytic activity of phenol over TCNQ@TiO_2 photocatalysts under the irradiation of (a) visible light ($\lambda > 450$ nm) and (b) UV light ($\lambda > 365$ nm); photoresponses of TCNQ@TiO_2 electrodes under the irradiation of (c) visible light ($\lambda > 450$ nm) and (d) UV light ($\lambda = 254$ nm) [Na_2SO_4] = 0.1 M.

was benzoquinone and the peak at 4.8 min was catechol. As the reaction proceeded, the peak of phenol became lower, whereas the peaks of the intermediate species (hydroquinol and benzoquinone) increased gradually. The peak of catechol appeared after four hours and the peak of lower fatty acid appeared after six hours, indicating that ring cleavage reaction has occurred. However, the oxidation ability of the holes injected into the VB of TiO_2 is not high enough to mineralize phenol completely. Fig. 2b shows the changes of phenol and its degradation products with time under UV irradiation. The peak at 2.4 and 3.05 min was lower fatty acid, the peak at 2.8 min was system peak, the peak at 3.4 min was hydroquinol and the peak at 3.75 min was resorcinol. As the reaction proceeded, the intensity of phenol peak was decreased with continuous UV irradiation, while the intensity of the intermediate products peaks (hydroquinol and resorcinol) increased gradually. The peak of lower fatty acid at 2.4 min down shifted by about 0.09 min, indicating that molecular mass of the degradation intermediates became smaller and phenol was degraded into small organic molecules.

3.2. Core–shell structure of TCNQ@TiO_2

The transmission electron microscopy (TEM) analysis is shown as Fig. 3a and b. The morphology of TiO_2 didn't change significantly and none of aggregation phenomenon was observed, which indicates that nano-size and morphology make little contribution to photocatalytic activity in this system. It can be seen from the SEM images (Fig. S1d) that TCNQ has bulk morphology, while no solid block was observed in TCNQ@TiO_2, indicating that TCNQ@TiO_2 is not a mechanical mixture and the morphology of TCNQ@TiO_2 is likely to be core–shell structure. The pore size distribution (Fig. S2) shows that the specific surface area of TCNQ@TiO_2 decreases gradually and the pore volume increases, respectively, with the increasing of the TCNQ loading amounts, indicating that the particle size is increasing gradually and TCNQ is coated on the surface of TiO_2.

Fig. 3c and d shows HRTEM images of TCNQ@TiO_2-20% photocatalyst. The red line shown in Fig. 3c was the crystal boundary of anatase and rutile. The inter-planar spacing above the crystal boundary is 0.351 nm, corresponding to the anatase (1 0 1) plane. The measured inter-planar spacing blow the crystal boundary is 0.248 nm, which corresponds to the rutile (1 0 1) plane. The lattice structure of TiO_2 was very orderly and the outer boundary of the as-prepared sample was distinctly different from the TiO_2 core. Distinct core–shell structure was formed and the thickness of the TCNQ layer coated on the TCNQ@TiO_2-20% sample was approximately 2 nm, corresponding to three TCNQ layers [36,37]. Suppose the TiO_2 particle is sphere and all the TCNQ was coated on the surface of TiO_2, the shell should be 3.8 nm. However, as the real TiO_2 particle is irregularly shaped and part of TCNQ was adsorbed on the surface of the vessel wall due to Coanda effect, the real thickness of TCNQ shell was about 2 nm.

Fig. 4a shows X-ray diffraction photometer (XRD) of TCNQ@TiO_2 photocatalysts with different loads. Diffraction peaks at 25.2° and 27.3° are the characteristic diffraction peaks of 101 lattice plane

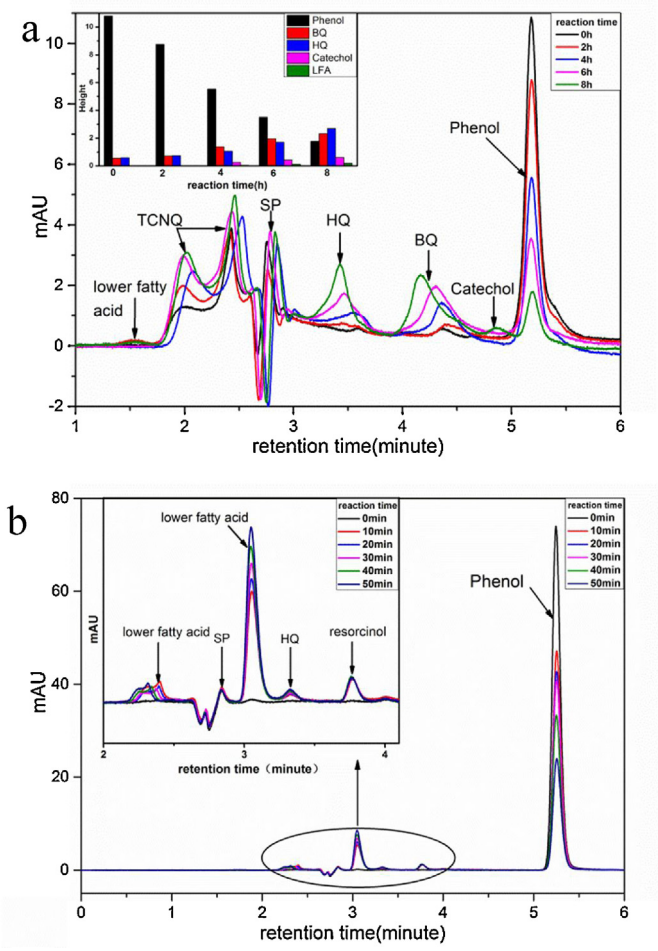

Fig. 2. Distribution of photocatalytic degradation species of phenol by (a) TCNQ@TiO_2-20% under visible light and (b) TCNQ@TiO_2-1% under UV irradiation.

of anatase and 110 lattice plane of rutile. The crystal structure of TiO_2 loading with different amounts of TCNQ did not change. There was no crystalline TCNQ in the TCNQ@TiO_2 photocatalysts with low TCNQ loading (<15%), whereas the as-prepared samples with higher TCNQ loading (>15%) exhibited crystalline TCNQ peaks (10.9°, 18.7°, 21.8°, 25.8°, 28.4° and 30.2°). The peak intensities increased with the increasing proportion of TCNQ. Thus, it can be inferred that TCNQ was dispersed uniformly on the TiO_2 surface with low TCNQ loadings. Crystalline TCNQ appeared when its loading amount exceeded a threshold value (15%). Since TiO_2 can only load a certain amount of TCNQ, part of the TCNQ formed bulk crystals rather than loading on the surface of TiO_2 when the proportion of TCNQ exceeded 20%. As interaction between this part of TCNQ and TiO_2 was too weak, the holes generated on the HUMO orbit of this part of TCNQ cannot be injected into VB of TiO_2, resulting in the decrease of visible activity when the proportion of TCNQ exceeded 20% (shown in Fig. 1a).

The UV–vis DRS spectra of TiO_2 and different mass ratios of TCNQ@TiO_2 photocatalysts are shown in Fig. 4b. As expected, a sharp fundamental absorption edge rises at 410 for TiO_2, while the absorption edge of TCNQ@TiO_2 exhibited an apparent redshift gradually with the increase of TCNQ loading. The absorption edge of TCNQ@TiO_2-20% was about 455 nm, indicating that absorption edge was expanded so as to make use of visible light. Charge transfer absorption peaks were observed at 600 nm and 850 nm and the absorption intensity was the strongest when the loading amount of TCNQ was 20%. When the proportion of TCNQ was over 20%, the intensity of charge transfer absorption peaks decreased gradually, which is concerned with the formation of bulk TCNQ. Since the HOMO orbit of TCNQ is lower than the CB of TiO_2, the photogenerated holes on the HOMO orbit of TCNQ can be injected into the CB of TiO_2, generating new charge transfer absorption peaks and bringing about visible light activity.

As known, the photocatalytic activity was determined by various factors, such as phase structure, crystalline size, surface area and pore size [38,39]. XRD pattern (shown in Fig. 4a) of TiO_2 showed no change before and after modification by TCNQ, indicating that the introduction of TCNQ did not influence the lattice structure of TiO_2. The surface area decreased with the loading of TCNQ (BET surface area of TiO_2 and TCNQ@TiO_2-20% was 47.48 and 38.99 $m^2\ g^{-1}$, shown in Fig. S2). Since the decrease of BET surface area is not beneficial for photocatalytic reaction, it can be inferred that the increase of photocatalytic activity for composite photocatalysts should be attribute to the interaction between the TCNQ layers and TiO_2 core, which promotes the separation efficiency of photongenerated carriers. The interaction between the TCNQ layers and TiO_2 core is characterized by FT-IR spectra and Raman spectra.

Fig. 5a shows the FT-IR spectra [40] of TiO_2 and various TCNQ@TiO_2 photocatalysts. In the FT-IR spectrum of TCNQ, 2220 cm^{-1} and 1540 cm^{-1} were attributable to the C≡N and C=C stretching vibration modes. Respectively, 3040 cm^{-1} were related to the C—H characteristic vibration of the benzene ring. The characteristic vibration of TCNQ at 2220 cm^{-1} and 1540 cm^{-1} nearly disappeared when TCNQ was loaded to TiO_2, which indicates that the bond strengths of C≡N and C=C were weakened, suggesting that there was a covalent bond between TCNQ and TiO_2. This interaction was beneficial to the charge migration and the stability of core–shell structure. The characteristic vibration of TiO_2 at 2350 cm^{-1} was gradually weakened with the increase of the TCNQ, which indicates that the bond strength of Ti—O was weakened and TiO_2 is combined with TCNQ by chemical bonds rather than mechanical mixing.

Fig. 5b shows the Raman spectra of TiO_2 and various TCNQ@TiO_2 photocatalysts. The Raman shifts at 333, 600 and 708 cm^{-1} arise from the lattice vibrational peaks of TCNQ crystal, corresponding to the $A_g\nu_9$ mode, $A_g\nu_8$ mode and $A_g\nu_7$ mode of TCNQ crystal [37]. TCNQ peaks at 333 cm^{-1}, 600 cm^{-1} and 708 cm^{-1} almost disappeared when coated on the surface of TiO_2, indicating that TCNQ shell was amorphous. The peak at 143 cm^{-1} was attributable to the lattice vibrational peaks of TiO_2 crystal, which moved to a lower wavenumber with the increase of TCNQ. The red shift of this band indicated that the bond strengths of Ti—O was weakened, suggesting that there was a covalent bond between the conjugated π bond of TCNQ and TiO_2 [20]. The interaction was concerned with the charge transfer absorption peaks and the red shift of the absorption sideband shown in Fig. 4b.

3.3. Mechanism

To reveal the photocatalytic mechanism, the main oxidative species in the photocatalytic process are detected through the trapping experiments of radicals using tBuOH [41] as hydroxyl radical scavenger, N_2 [42] as superoxide radical scavenger and formic acid [43] as holes radical scavenger. As shown in Fig. 6a, the photocatalytic activity of TCNQ@TiO_2 under visible irradiation decreases obviously with the addition of holes scavenger (formic acid) and reduced slightly with the addition of hydroxyl radical scavenger (tBuOH) and superoxide radical scavenger (N_2), indicating that holes radicals are the main oxidative species while hydroxyl radicals and superoxide radicals are not the main oxidative species.

On the basis of the above analysis, a possible mechanism for the degradation of phenol under visible irradiation is proposed, as shown in Fig. 6b. Photogenereted electrons and holes are generated on the HOMO and LUMO of TCNQ when irradiated by visible light.

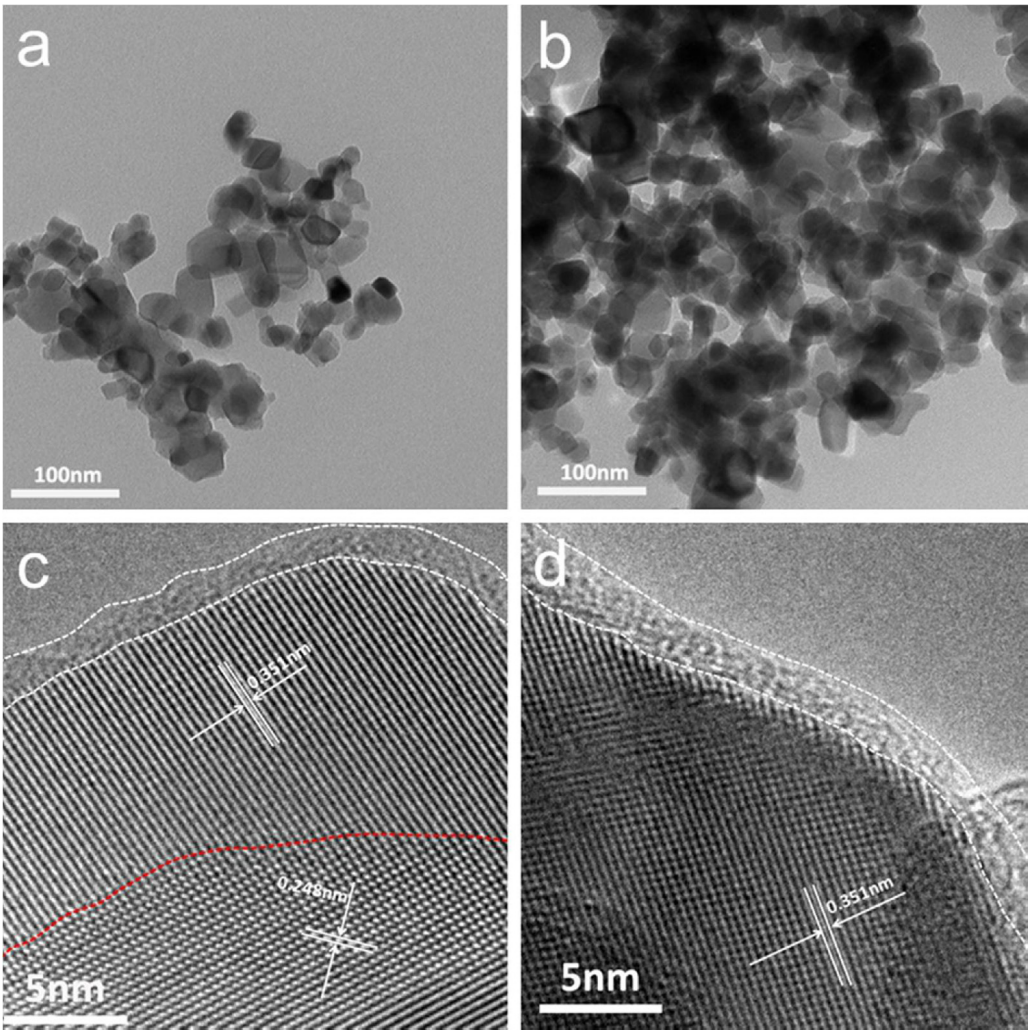

Fig. 3. TEM images of (a) TiO_2 and (b) TCNQ@TiO_2-20%; HRTEM images of (c) (d) TCNQ@TiO_2-20%.

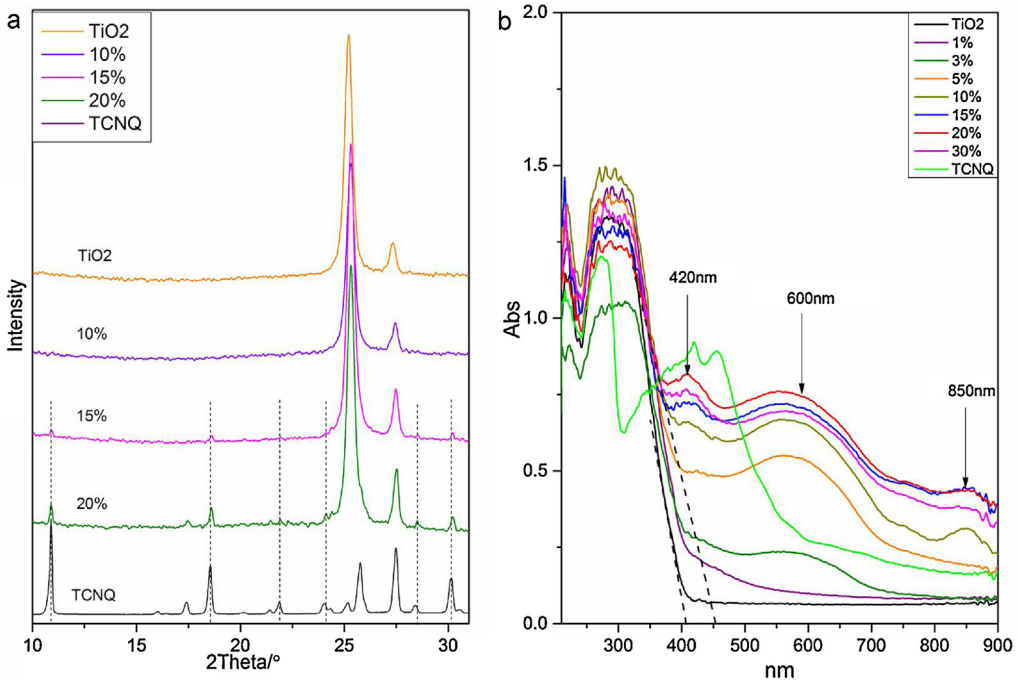

Fig. 4. (a) XRD patterns of TCNQ@TiO_2 photocatalysts and (b) Diffuse reflectance absorption spectra.

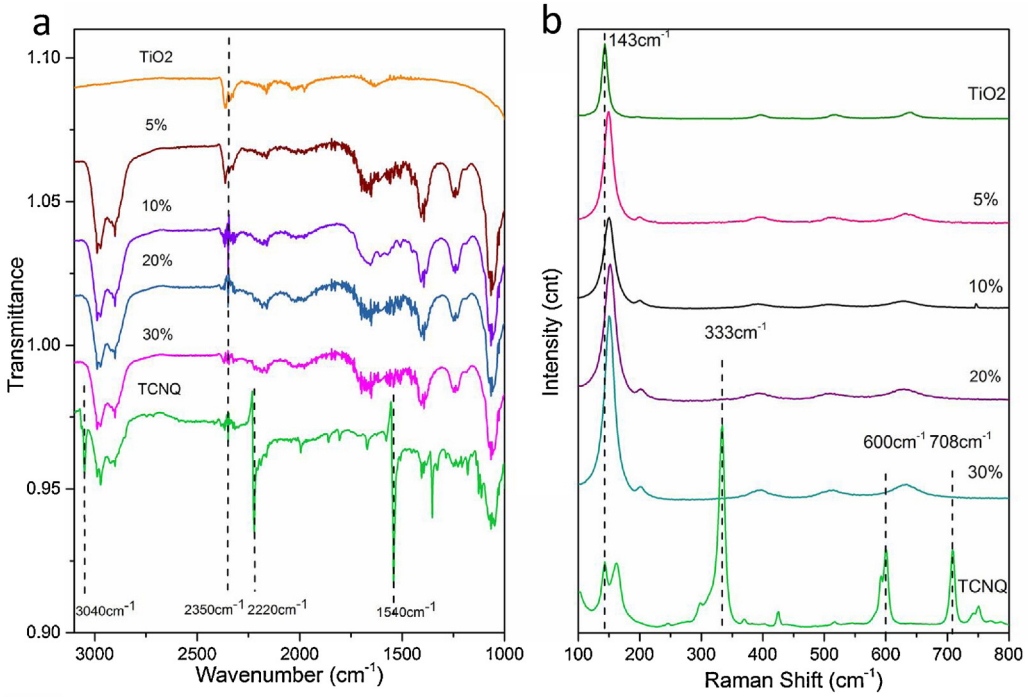

Fig. 5. (a) FTIR and (b) Raman spectra of TCNQ@TiO_2 photocatalysts.

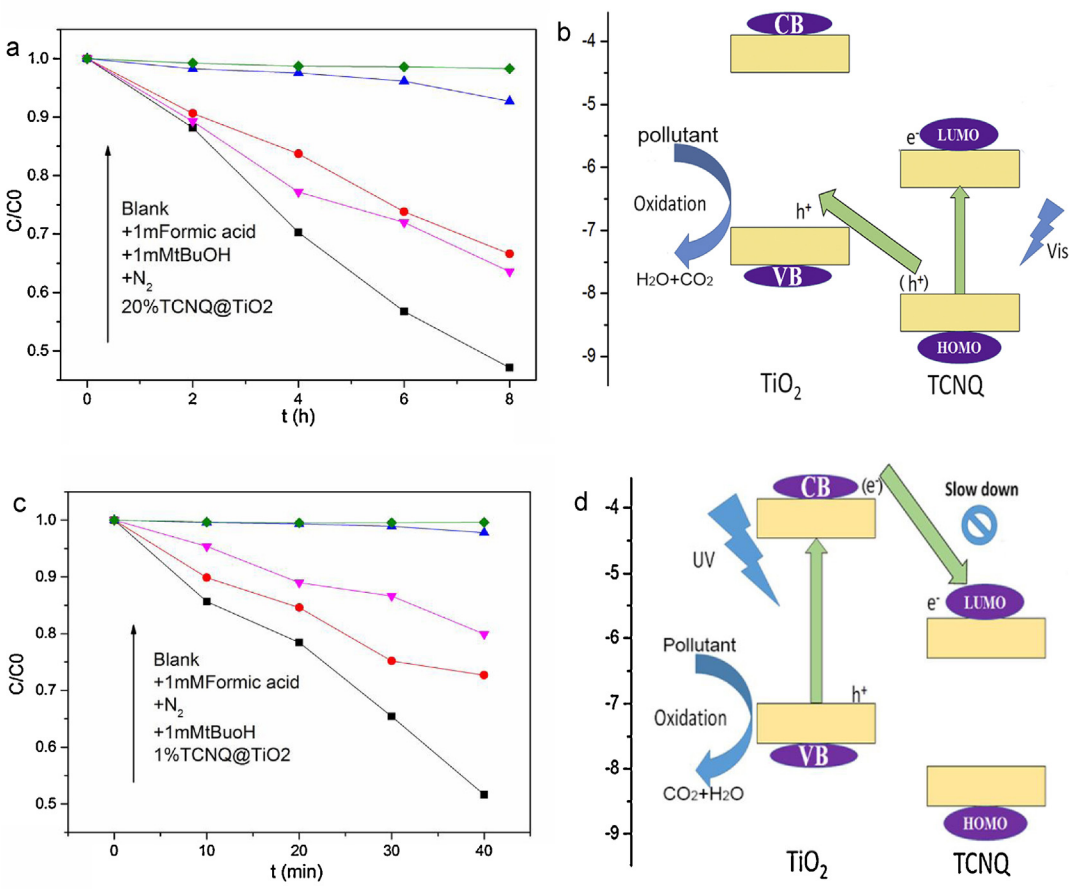

Fig. 6. The plots of photogenerated carriers trapping in the system of photodegradation of phenol by (a) TCNQ@TiO_2-20% under visible light and by (c) TCNQ@TiO_2-1% under UV light; Mechanism plots under (b) visible light and (d) UV light.

As the HOMO orbit of TCNQ is lower than the VB of TiO_2 [4,44], the photogenerated holes on the HOMO of TCNQ could be injected easily into the VB of TiO_2. The holes injected into the VB of TiO_2 could oxide organic pollutant directly, which contributes to the dramatic visible activity of TCNQ@TiO_2 photocatalyst in phenol degradation. However, the oxidation ability of the holes injected into the VB of TiO_2 is not high enough, so the phenol cannot be mineralized completely (shown in Fig. 2a). The interface charge separation efficiency of photogenerated electrons and holes is a crucial factor for photocatalytic activity. The interface charge separation efficiency under UV irradiation can be investigated by the typical electrochemical impedance spectra (presented as Nyquist plots) [45] and the smaller arc radius implies the higher charge transfer. The typical electrochemical impedance spectra (presented as Nyquist plots) under visible irradiation are shown in Fig. S3a. It is observed that the arc radius of TCNQ@TiO_2 becomes smaller with the increase of the proportion of TCNQ when the proportion of TCNQ was under 20%. This result demonstrates that the introduction of TCNQ enhances the separation and transfer efficiency of photogenerated carriers, which contributes to the enhancement of the visible light activity. When the proportion of TCNQ was over 20%, bulk crystals of TCNQ was formed (shown in Fig. 4a). The interaction between this part of TCNQ and TiO_2 was too weak that the holes generated on the HUMO orbit of TCNQ cannot be injected into VB of TiO_2, resulting in the decrease of photocatalytic activity.

As shown in Fig. 6c, the photocatalytic activity of TCNQ@TiO_2 under UV irradiation decreases obviously with the addition of holes scavenger (formic acid) and reduced slightly with the addition of hydroxyl radical scavenger(tBuOH) and superoxide radical scavenger(N_2), indicating that holes radicals are the main oxidative species while hydroxyl radicals and superoxide radicals are not the main oxidative species. According to Fig. 2b and Fig. S4, the degradation species of TiO_2 and TCNQ@TiO_2 were almost the same under UV irradiation, suggesting that the reaction mechanisms of TiO_2 and TCNQ@TiO_2 are the same under UV irradiation.

On the basis of the above analysis, a possible mechanism for the degradation of phenol under UV irradiation is proposed, as shown in Fig. 6d. When irradiated by UV light, photogenerated electrons and holes are generated on the CB and VB of TiO_2. As the CB position of TiO_2 is higher than the lowest unoccupied molecular orbital (LUMO) of TCNQ [4,44], the photogenerated electrons on the CB of TiO_2 could be injected easily to the LUMO orbit of TCNQ. However, the LUMO orbit of TCNQ is too low that electrons could not combine with O_2 easily, which interdicts the formation of superoxide radicals. With the increase of TCNQ, almost all the electrons were injected into LUMO orbit of TCNQ, inhibiting the separation of photoinduced carriers and reducing the intrinsic activity of TiO_2 under UV irradiation. The typical electrochemical impedance spectra (presented as Nyquist plots) under UV irradiation are shown in Fig. S3b. It is observed that the arc radius of TCNQ@TiO_2 is larger than that of TiO_2 with and without UV irradiation, indicating less charge transfer efficiency of TCNQ@TiO_2. This result demonstrates that the introduction of TCNQ to TiO_2 hinders the separation and transfer efficiency of photogenerated carriers, which results in the decrease of the UV light activity.

4. Conclusion

TCNQ@TiO_2 photocatalyst with core–shell structure was synthesized. This photocatalyst showed an excellent visible activity. The visible activity comes from the injection of the photogenerated holes on the HOMO of TCNQ into the VB of TiO_2 under visible light irradiation. The holes injected into the VB of TiO_2 could oxidize organic pollutant directly, but it cannot mineralize phenol completely.

Acknowledgements

This work was partly supported by National Basic Research Program of China (973 Program) (2013CB632403), National High Technology Research and Development Program of China (2012AA062701) and Chinese National Science Foundation (21373121).

Appendix A. Supplementary data

Supplementary material related to this article can be found, in the online version, at http://dx.doi.org/10.1016/j.apcatb.2014.04.050.

References

[1] S. Ardizzone, C.L. Bianchi, G. Cappelletti, S. Gialanella, C. Pirola, V. Ragaini, J. Phys. Chem. C 111 (2007) 13222–13231.
[2] A. Fujishima, K. Honda, Nature 238 (1972) 37–38.
[3] S.N. Frank, A.J. Bard, J. Phys. Chem. 81 (1977) 1484–1488.
[4] S.U.M. Khan, M. Al-Shahry, W.B. Ingler, Science 297 (2002) 2243–2245.
[5] N. Serpone, J. Phys. Chem. B 110 (2006) 24287–24293.
[6] H. Zhang, R. Zong, J. Zhao, Y. Zhu, Environ. Sci. Technol. 42 (2008) 3803–3807.
[7] V. Iliev, J. Photochem. Photobiol., A: Chem. 151 (2002) 195–199.
[8] J. Moon, C.Y. Yun, K.-W. Chung, M.-S. Kang, J. Yi, Catal. Today 87 (2003) 77–86.
[9] T. Peng, K. Dai, H. Yi, D. Ke, P. Cai, L. Zan, Chem. Phys. Lett. 460 (2008) 216–219.
[10] D. Dvoranová, V. Brezová, M. Mazúr, M.A. Malati, Appl. Catal., B: Environ. 37 (2002) 91–105.
[11] K. Lee, N.H. Lee, S.H. Shin, H.G. Lee, S.J. Kim, Mater. Sci. Eng., B 129 (2006) 109–115.
[12] M. Sathish, B. Viswanathan, R.P. Viswanath, C.S. Gopinath, Chem. Mater. 17 (2005) 6349–6353.
[13] K. Nagaveni, M.S. Hegde, N. Ravishankar, G.N. Subbanna, G. Madras, Langmuir 20 (2004) 2900–2907.
[14] S. Sakthivel, H. Kisch, Angew. Chem., Int. Ed. 42 (2003) 4908–4911.
[15] M. Shen, Z. Wu, H. Huang, Y. Du, Z. Zou, P. Yang, Mater. Lett. 60 (2006) 693–697.
[16] B. Zhang, W. Zou, J. Zhang, Res. Chem. Intermed. (2013) 1–14, http://dx.doi.org/10.1007/s11164-013-1422-7.
[17] F. Chen, W. Zou, W. Qu, J. Zhang, Catal. Commun. 10 (2009) 1510–1513.
[18] W. Zou, J. Zhang, F. Chen, Mater. Lett. 64 (2010) 1710–1712.
[19] W. Zou, J.-L. Zhang, F. Chen, M. Anpo, D.-N. He, Res. Chem. Intermed. 35 (2009) 717–726.
[20] Y. Wang, R. Shi, J. Lin, Y. Zhu, Appl. Catal., B: Environ. 100 (2010) 179–183.
[21] L. Zhang, Y. Wang, T. Xu, S. Zhu, Y. Zhu, J. Mol. Catal. A: Chem. 331 (2010) 7–14.
[22] A.R. Malagutti, H.A.J.L. Mourão, J.R. Garbin, C. Ribeiro, Appl. Catal., B: Environ. 90 (2009) 205–212.
[23] T. Sasaki, N. Koshizaki, J.-W. Yoon, K.M. Beck, J. Photochem. Photobiol., A: Chem. 145 (2001) 11–16.
[24] Y. Tian, T. Tatsuma, J. Am. Chem. Soc. 127 (2005) 7632–7637.
[25] i.I Garcia-Yoldi, J.S. Miller, J.J. Novoa, J. Phys. Chem. A 113 (2008) 484–492.
[26] C. Hong, P. Yan, Q. Li, G. Hou, G. Li, J. Organomet. Chem. 739 (2013) 45–51.
[27] J. Ferraris, D.O. Cowan, V. Walatka, J.H. Perlstein, J. Am. Chem. Soc. 95 (1973) 948–949.
[28] Y. Washino, K. Murata, M. Ashizawa, S. Kawauchi, T. Michinobu, Polym. J. 43 (2011) 364–369.
[29] N. Yoshioka, H. Nishide, K. Inagaki, K. Inagaki, E. Tsuchida, Polym. Bull. 23 (1990) 631–636.
[30] S. Inagi, K. Naka, Y. Chujo, J. Mater. Chem. 17 (2007) 4122–4135.
[31] B. Li, H. Cao, J. Mater. Chem. 21 (2011) 3346–3349.
[32] T. Xu, L. Zhang, H. Cheng, Y. Zhu, Appl. Catal., B: Environ. 101 (2011) 382–387.
[33] Y. Yang, L. Ren, C. Zhang, S. Huang, T. Liu, ACS Appl. Mater. Interfaces 3 (2011) 2779–2785.
[34] X. Bai, L. Wang, R. Zong, Y. Lv, Y. Sun, Y. Zhu, Langmuir 29 (2013) 3097–3105.
[35] Y. Wang, R. Shi, J. Lin, Y. Zhu, Energy Environ. Sci. 4 (2011) 2922–2929.
[36] R.E. Long, R.A. Sparks, K.N. Trueblood, Acta Crystallogr. 18 (1965) 932–939.
[37] Z.P. Hu, Z.X. Shen, L. Qin, S.H. Tang, M.H. Kuok, G.Q. Xu, K.F. Mok, H.H. Huang, J. Mol. Struct. 356 (1995) 163–168.
[38] J.C. Yu, J. Yu, L. Zhang, W. Ho, J. Photochem. Photobiol., A: Chem. 148 (2002) 263–271.
[39] J.C. Yu, J. Yu, W. Ho, L. Zhang, Chem. Commun. 19 (2001) 1942–1943.
[40] J.S. Chappell, A.N. Bloch, W.A. Bryden, M. Maxfield, T.O. Poehler, D.O. Cowan, J. Am. Chem. Soc. 103 (1981) 2442–2443.
[41] H. Lee, W. Choi, Environ. Sci. Technol. 36 (2002) 3872–3878.
[42] C. Pan, Y. Zhu, Environ. Sci. Technol. 44 (2010) 5570–5574.
[43] T. Tan, D. Beydoun, R. Amal, J. Photochem. Photobiol., A: Chem. 159 (2003) 273–280.
[44] N. Martín, J.L. Segura, C. Seoane, J. Mater. Chem. 7 (1997) 1661–1676.
[45] W. Leng, Z. Zhang, J. Zhang, C. Cao, J. Phys. Chem. B 109 (2005) 15008–15023.